Title
Spectral phasor approach for fingerprinting of photo-activatable fluorescent proteins Dronpa, Kaede and KikGR.

Journal
Methods and Applications in Fluorescence, 1(3)

ISSN
2050-6120

Authors
Cutrale, Francesco
Salih, Anya
Gratton, Enrico

Publication Date
2013

DOI
10.1088/2050-6120/1/3/035001

Spectral phasor approach for fingerprinting of photo-activatable fluorescent proteins Dronpa, Kaede and KikGR

2013 Methods Appl. Fluoresc. 1 035001

(http://iopscience.iop.org/2050-6120/1/3/035001)

Methods Appl. Fluoresc. **1** (2013) 035001 (10pp) doi:10.1088/2050-6120/1/3/035001

Spectral phasor approach for fingerprinting of photo-activatable fluorescent proteins Dronpa, Kaede and KikGR

Francesco Cutrale[1], **Anya Salih**[2] **and Enrico Gratton**[1]

[1] Laboratory of Fluorescence Dynamics, Biomedical Engineering Department, University of California, Irvine, CA 92697, USA
[2] School of Science and Health, University of Western Sydney, Australia

E-mail: egratton@uci.edu

Received 20 December 2012, in final form 16 February 2013
Published 4 June 2013
Online at stacks.iop.org/MAF/1/035001

Abstract
The phasor global analysis algorithm is common for fluorescence lifetime applications, but has only been recently proposed for spectral analysis. Here the phasor representation and fingerprinting is exploited in its second harmonic to determine the number and spectra of photo-activated states as well as their conversion dynamics. We follow the sequence of photo-activation of proteins over time by rapidly collecting multiple spectral images. The phasor representation of the cumulative images provides easy identification of the spectral signatures of each photo-activatable protein.

1. Introduction

The phasor approach to fluorescence lifetime imaging microscopy (FLIM) (Digman *et al* 2008) is gaining widespread use in the microscopy and spectroscopy community. This powerful technique overcomes the complication of exponential component analysis in FLIM by introducing a fit-free approach. Traditional FLIM analysis uses global fitting procedures which could be difficult to interpret when many exponential components are present. Instead, the phasor approach produces instantaneous, global and quantitative results. In other words, phasors provide a simplified representation of the data, leading to a logical easy graphical interpretation of the various fluorescent species without *a priori* assumptions about their number and spectra.

Applications of the FLIM phasor approach to live cells span from calcium gradient measurement (Celli *et al* 2010, Sanchez *et al* 2011) to a Na-dependent phosphate transporter (Giral *et al* 2012, 2011) and Förster resonance energy transfer detection in biosensors (Hinde *et al* 2012). The work of Stringari (2011, 2012) further exploits this approach by fingerprinting a large number of optical biomarkers with unique lifetime phasor locations. The wide range of applications here listed underlines the usefulness of the method.

The potential of the phasor method was further expanded by the recent work of Fereidouni (2012). This work describes the use of phasors for (hyper-) spectral imaging, hence translating the simplified representation of the phasor plot from the lifetime domain to the wavelength representation. The recent availability of hyper-spectral cameras and the implementation of spectral scan in confocal microscopes could increase datasets size n-fold, with n equal to the number of spectral channels available. This larger dataset necessitates a practical representation method capable of resolving the complexity of multispectral analysis with a simple logical interpretation. Spectral phasors are one appealing solution to this issue.

In this work we apply the spectral phasor approach to follow the dynamics of photo-activatable fluorescent proteins (FPs). This field of application is particularly important because the number and the spectra of the various states that can be obtained by photo-activation are not necessarily known. Of course there are several methods based on

spectral demixing and principal component analysis that can deal with this situation, but the spectral phasor approach provides a particularly simple, visual and fit-free approach for large datasets while maintaining commercial microscope compatibility. The recent development of molecular reporters including genetically encoded proteins started with the introduction of the green fluorescent protein (GFP). Because of the efforts of multiple laboratories, identification, development and enhancement of novel proteins covering the entire visible spectrum has been achieved. The development of photo-activatable fluorescent proteins (PA-FPs) adds color switching capability to the probes, opening the path to super-resolution techniques such as photo-activated localization microscopy (Betzig *et al* 2006).

PA-FPs are particular FPs that can change spectral properties upon irradiation with a specific wavelength. This change in color can be irreversible or reversible (Chudakov *et al* 2010). Kaede (Ando *et al* 2002) belongs to the class of irreversible PA-FPs. It switches from green to red when illuminated with UV light, shifting the emission maximum from 518 to 582 nm. In the same class is Kikume Green–Red (KikGR) (Tsutsui *et al* 2005) converting from a green form at 517 nm to red at 593 nm with UV photoconversion.

Dronpa (Ando *et al* 2004, Habuchi *et al* 2005, 2006) is a reversible photo-switchable protein that goes from a mature state of green fluorescence (518 nm) to a dark state. The emission at 518 nm can be evoked using UV light (405 nm) and returned to the 'dark' state by continuous excitation with a 488 nm laser.

Here we present an approach to photo-activatable fluorescent protein mapping using the spectral phasor approach. To demonstrate our approach we use a large NiT agarose bead uniformly coated with the PA-FP. We then photo-activate different regions of the bead to form an image of regions with different levels of photoconversion. We follow the conversion in time of the various regions. The results are presented as sequences of images. The spectrum in each pixel of the image is analyzed using the spectral phasor method. Using this method we can clearly distinguish the various regions of activation and quantify the activation kinetics. For all proteins investigated we detected only two states. We then mixed PA-FPs and we show that we can quantitatively follow the simultaneous activation of proteins in a mixture. In the case of proteins with multiple intermediate steps, this method could allow the separation of these states and quantification of their relative amounts. If in the cell there are regions in which the photoconversion can be altered by the cell environment, we could directly map where these processes occur. These intermediate steps or altered states of conversion would not belong to the linear combinations of PA-FP green–red states, showing up in the spectral phasor plot as vertices outside the line connecting two colors.

2. Material and methods

2.1. Protein expression, purification and sample preparation

Kaede, KikGR and Dronpa plasmids were expressed in *Escherichia coli* BL21(DE3) bacterial cultures with pRSET vector. A selected bacterial colony was inoculated overnight at 37 °C at 250 rpm in Luria broth with 100 μg ml^{-1} ampicillin until reaching optical density 0.8. 0.5 mM IPTG (isopropyl beta-D-1-thiogalactopyranoside) was added to induce protein expression. The solution was incubated for 4 h at 37 °C, 250 rpm and cells were harvested by centrifugation at 4100 rpm and 4 °C for 15 min. Harvested cells were resuspended using a lysis buffer (20 mM Tris, 1% Triton, 1 mM PMSF (phenylmethanesulfonylfluoride) and 10 μg ml^{-1} leupeptin). Cells were subsequently sonicated for ten cycles, 10 s on and 50 s, off incubated on ice, ultra-centrifuged at 20 000 rpm and 4 °C for 30 min and filtered with a syringe driven filtering unit (Millex GP filter unit, 0.22 μm, Merck Millipore, Darmstadt, Germany). Filtrate was incubated in ice for 1 h at 100 rpm with 1 ml Ni-NTA agarose gel (Qiagen, Hilden, Germany) and run through purification columns (Illustra NAP-5 Sephadex G-25 columns, GE Healthcare, Buckinghamshire, UK) previously equilibrated with buffer (20 mM Tris, 0.5 M NaCl). The column was washed with 10 ml washing buffer (20 mM Tris, 300 mM NaCl, 20 mM imidazole, 50 mM KH_2PO_4, potassium phosphate monobasic) and subsequently eluted (20 mM Tris, 300 mM NaCl, 300 mM imidazole, 50 mM KH_2PO_4, potassium phosphate monobasic). The eluate was washed with 20 ml 20 mM Tris and concentrated in centrifugal filter (Amicon Ultra-15 centrifugal filters, Merck Millipore, Darmstadt, Germany).

Samples were prepared by selecting a region of interest of approximately 20 mm $\times$ 25 mm on a coverslip using a Liquid Blocker Super Pap pen (Daido Sangyo, Saitama, Japan). 1 μl Ni-NTA agarose beads (Qiagen, Hilden, Germany), previously washed with 20 mM Tris buffer, was added in the center of the delimited region. 1 μl of protein solution was added on top. A 24 mm $\times$ 30 mm cover glass is used to cover the sample and sealing is performed using nail polish. Contact between acetone contained in the sealer and the liquid blocker region was carefully avoided, preserving the protein contained in the center of the slide from chemical alteration and desiccation.

2.2. Imaging

Samples were imaged using LSM 710 Meta (Zeiss, Jena, Germany) with standard OEM diode lasers, 405 nm and 561 nm, respectively yielding 5.25 μW and 111.4 μW maximum power at the sample. We used a 488 nm Lasos RMC 7812 Z1 (Lasos Lasertechnik, Jena, Germany) Arg-ion laser with 6.02 μW power at the sample. The laser power was measured on the objective using a standard power meter. The duty cycle of illumination was determined by a fast photo-diode and included in the calculation of the laser power. The objective used was a Plan-Apochromat 63 $\times$ /1.40 oil DIC M27 (Zeiss, Jena, Germany). The images were acquired in the spectral mode of the Zeiss 710 using 32 channels covering the spectrum from 416.32 to 727.65 nm with 9.73 nm bandwidth per channel. All images were acquired using a pixel dwell time of 12.6 μs and 256 $\times$ 256 pixel size frames. After focusing on one of

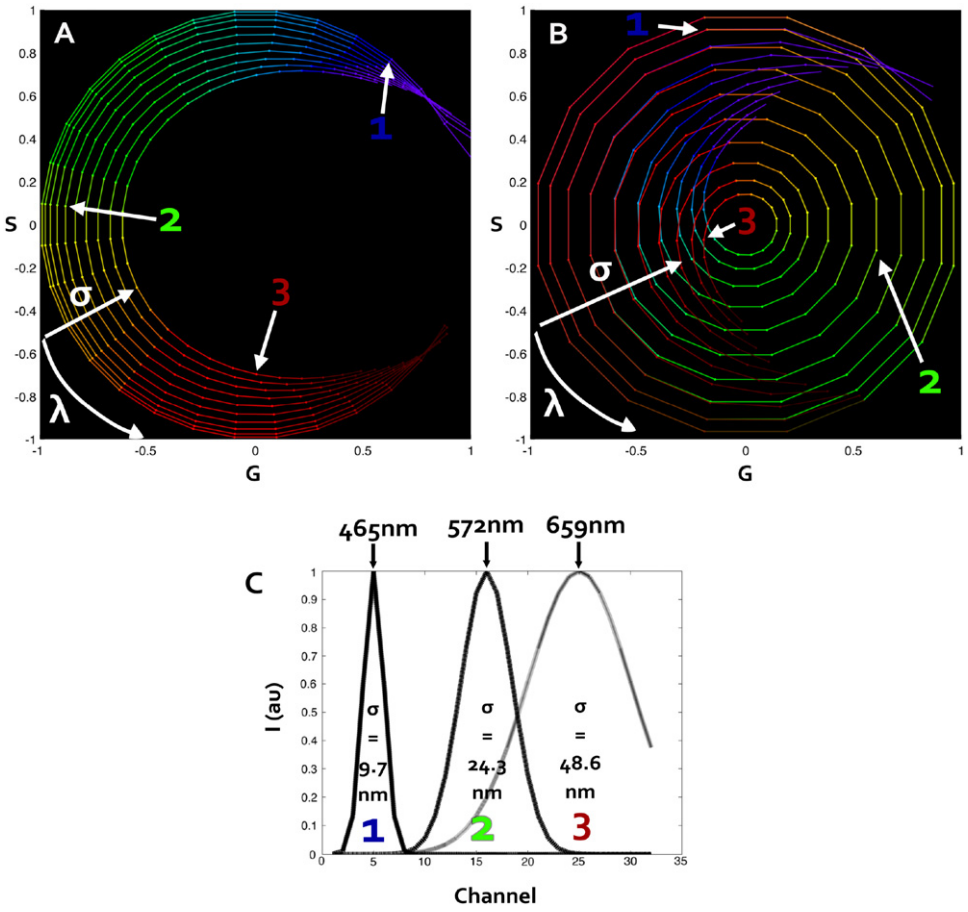

Figure 1. First harmonic (A) and second harmonic (B) spectral phasor. The dataset used was simulated using 32 wavelength channels and a Gaussian spectrum changing in both position and width. The color coding is representative of the corresponding wavelength. (C) Three of the simulated spectra used for calculating (A) and (B). The corresponding points in the spectral phasor plot are marked in both first and second harmonics. The change in wavelength peak changes the position counterclockwise on the spectral plot. An increase in the width of the spectrum will shift the point toward the origin of the axes.

the protein-bound agarose beads, three regions of interest (ROIs) were selected on the bead, approximately of the same size. These regions were photo-activated with different laser intensities over time. After each photo-activation step, one spectral image was acquired. This method allows for a step-by-step photoconversion monitoring with time resolution that depends on the amount of energy deployed on the ROI. Software used for the photo-activation is Zen 2009, selecting 'bleaching' mode in parallel with 'time series' and 'regions'. Spectra were collected at 1 frame s^{-1}.

2.3. Spectral phasor calculation

Spectral phasors were calculated starting from the equations for the phasor transformation published by Digman *et al* (2008) and recently adapted to the spectral phasors by Fereidouni (2012). The equations of $G_i(\lambda)$ and $S_i(\lambda)$ for each image i were modified for a discrete case as follows:

$$G_i(\lambda) = \frac{\sum_{\lambda=\lambda_s}^{\lambda_f} I(\lambda) \cos(n\omega\lambda)\,\Delta\lambda}{\sum_{\lambda=\lambda_s}^{\lambda_f} I(\lambda)\,\Delta\lambda} \tag{1}$$

$$S_i(\lambda) = \frac{\sum_{\lambda=\lambda_s}^{\lambda_f} I(\lambda) \sin(n\omega\lambda)\,\Delta\lambda}{\sum_{\lambda=\lambda_s}^{\lambda_f} I(\lambda)\,\Delta\lambda} \tag{2}$$

where λ_s and λ_f are the starting wavelength and the final wavelength of the spectrum, n is the harmonic number, and $\omega = 2\pi f$ with the frequency $f = (n \times \text{spectral channels})^{-1}$.

The datasets acquired are spectral images of 32 channels over time. A cumulative plot of all the $G_i(\lambda)$ and $S_i(\lambda)$ coordinates provides an overall visualization of spectral changes in time. Therefore,

$$\text{phasor plot}(G,S) = \begin{cases} \sum_i \text{hist}\,(G_i(\lambda)) \\ \sum_i \text{hist}\,(S_i(\lambda))\,. \end{cases} \tag{3}$$

In words, the phasor plot used in this paper is the sum of the $(G_i(\lambda)\,, S_i(\lambda))$ histograms of pixels of each spectral image belonging to the time series acquisition. Data analysis was performed using the SimFCS program (www.lfd.uci.edu). As shown in equations (1) and (2), the spectral transformation can be done at a harmonic number n. An example of a first and second harmonic spectral phasor is illustrated in figure 1.

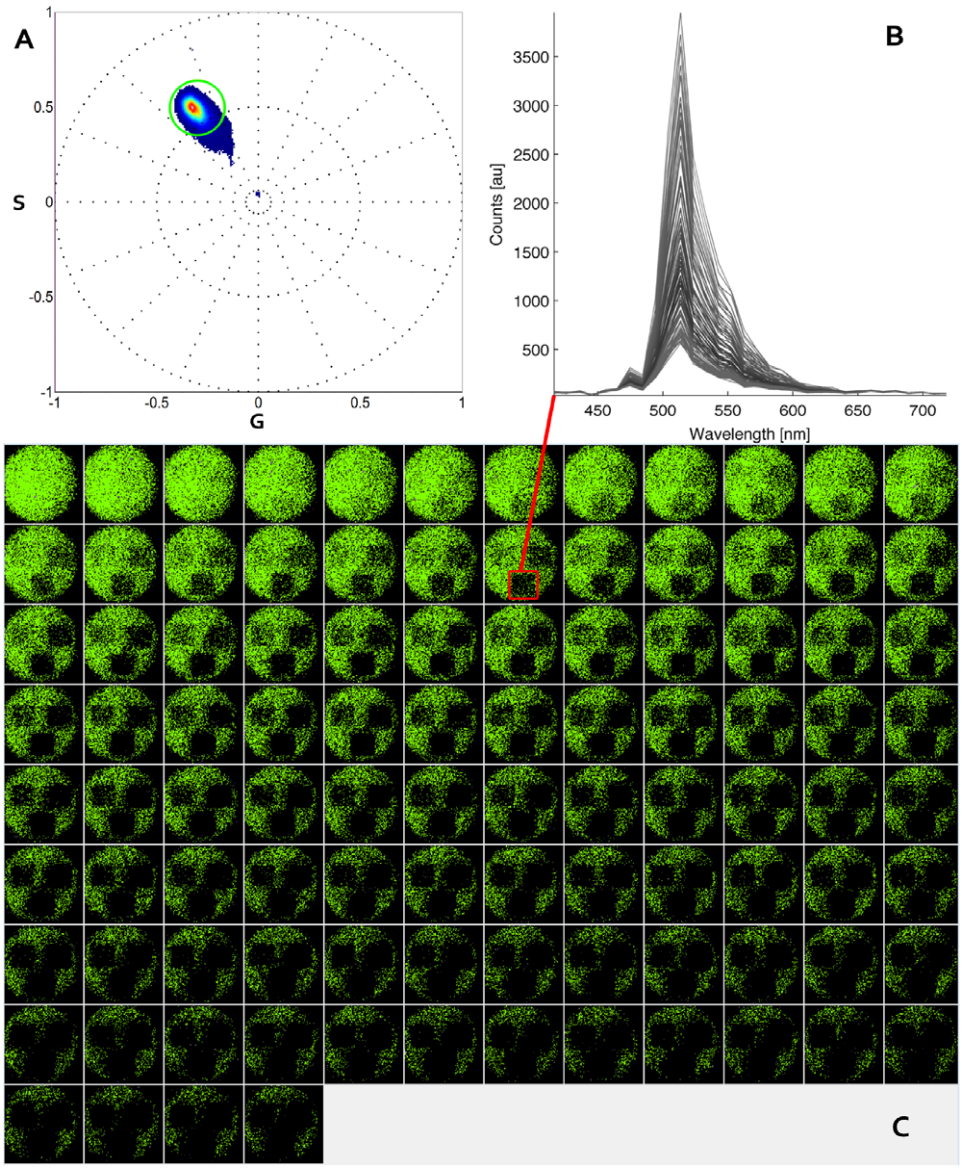

Figure 2. Dronpa converts from fluorescent (511 nm) to dark upon photo-activation. (A) First harmonic spectral phasor analysis. Three ROIs are selected on the bead on areas of 68 × 70 pixels. The laser power at 488 nm is set respectively at 1.42 μW (left ROI), 2.66 μW (right ROI) and 4.38 μW (bottom ROI). The zoom is set at 2.2 with a frame size of 61.10 μm. 100 frames are acquired using 488 nm wavelength at 1 s/frame. (C) The points selected by the cursor in the phasor plot (A) are colored with the cursor color. One ROI with 4.38 μW, 488 nm laser photo-activation is selected for the entire sequence to produce the spectral graph (B), where the time series is represented in grayscale.

We simulated an acquisition with 32 channels covering the spectra from 416 to 727 nm and plotted a color coded graph representative of the wavelength simulated. The same dataset is used to calculate first and second harmonics. In a simple comparison, it can be noted that the first harmonic covers an angle of $3/4\pi$ radians. The second harmonic, instead, circles over 4π radians, overlapping from the orange region (580.9 nm) to the deep red (720 nm). As a consequence, data are more distributed and linearly positioned compared to the first harmonic. The overlap does not affect the analysis, since spectral phasor properties of linearity and orthogonality are still respected at all harmonics. The utility of the spectral phasor approach is greatly expanded by the use of the second harmonic. The wider range and increased linearity facilitate the understanding of the dataset. Furthermore, the higher harmonic allows a marked distinction between two peaks in the spectra, matching the typology of data from photo-activatable proteins. This higher sensitivity arises from equations (1) and (2), where the shorter period of the sine and cosine amplifies differences in the spectrum.

3. Results and discussion

The application of spectral phasors in this work makes use of three commonly used PA-FPs, Dronpa, Kaede and KikGR. We acquired separate spectral sequences of photo-activation for

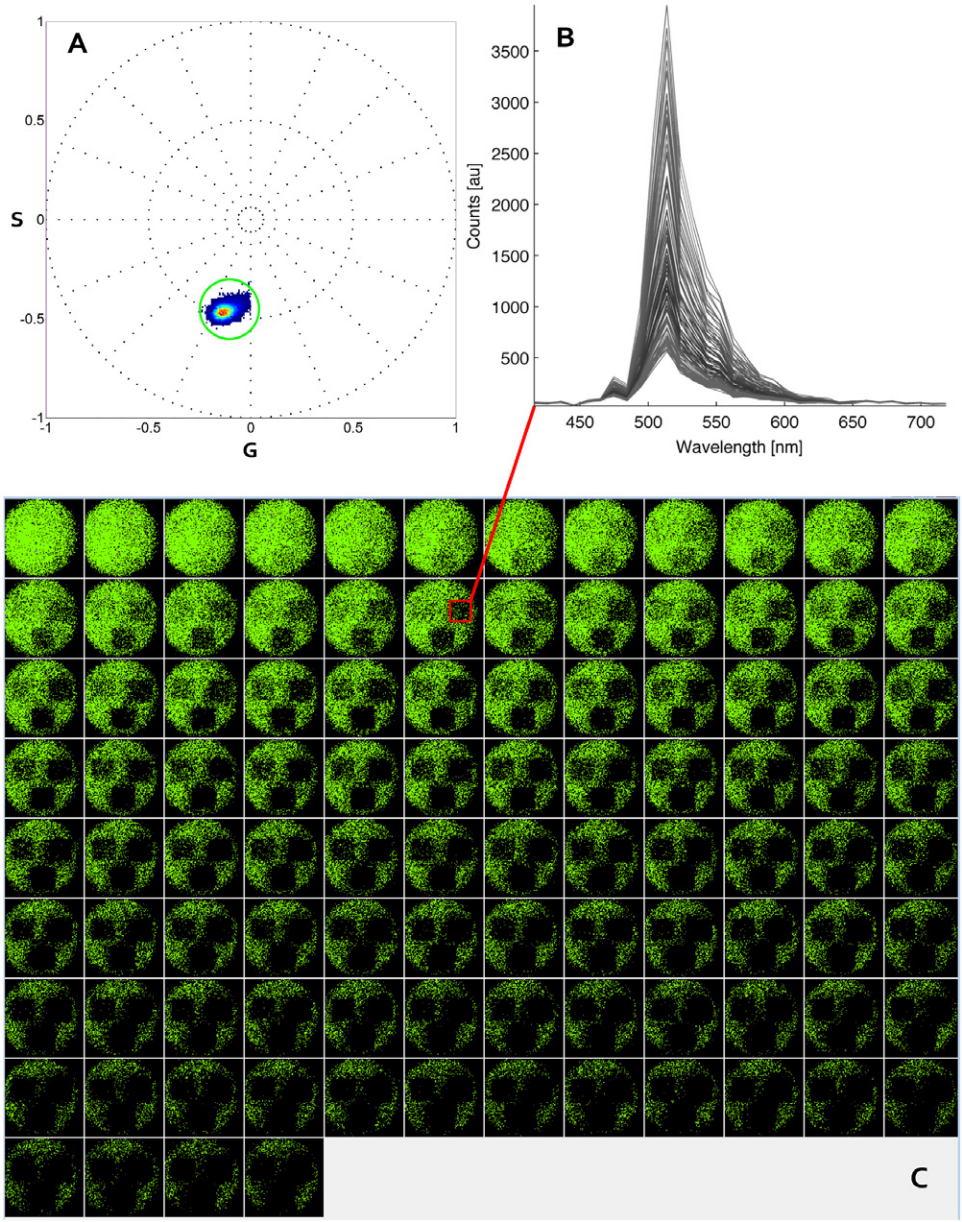

Figure 3. Dronpa converts from fluorescent to dark upon illumination. (A) Second harmonic spectral phasor analysis. The same dataset as used in figure 1 is analyzed using the second spectral harmonic. (C) The points selected by the cursor in the phasor plot (A) are colored with the cursor color on a grayscale image sequence. The ROI with 2.66 μW, 488 nm laser photo-activation is selected on all frames to produce the spectral graph (B).

each protein and calculated the resulting cumulative spectral phasor.

3.1. DRONPA

We added Dronpa at a concentration of 30.3 mg ml^{-1} to the Ni-NTA beads until the binding sites were saturated. Imaging of Dronpa started from the fluorescent state, sequentially inactivating the protein in three ROIs with different 488 nm laser powers. The spectral phasor of 60 images for first and second harmonics is shown in figure 2. First harmonic analysis provides a neat separation of Dronpa in the active state (green), intermediate (blue, seen only in the spectrum plot) and inactive state, which is the dot at the center of the phasor plot and in red in the spectrum panel. The Dronpa 'dark' state is located at the central position of the plot as expected from equations (1) and (2). The dark spectrum has no particular phase and it is not modulated (very broad). We cannot distinguish the 'dark' state of the protein from the background. A circle-shaped cursor is used to select areas of interest on the spectral phasor plot. The points selected are colored with the same color as the cursor in the image. The color of the cursor (green) is used to paint all pixels in the image that have their phasor positions selected by the cursor. Second harmonic analysis provides visually complete information of the photo-activation pattern. The major phasor

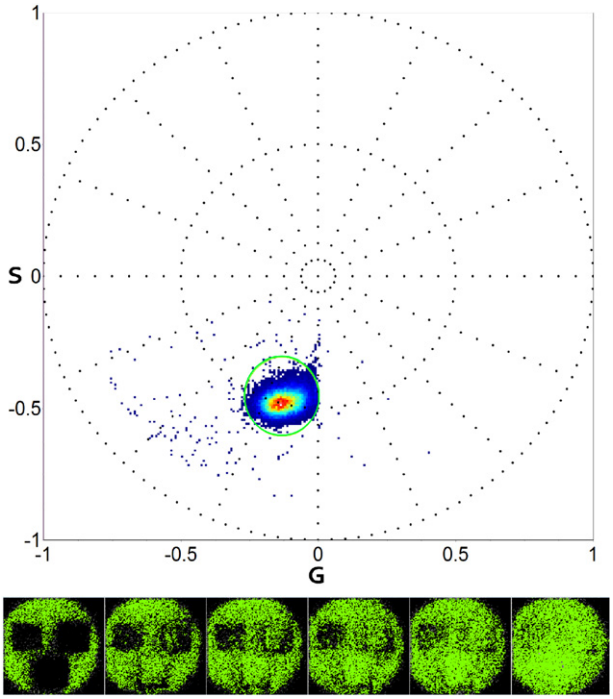

Figure 4. Dronpa dark-to-fluorescent photo-activation (top). After converting Dronpa to the 'dark' state in figures 2 and 3 the same sample is used for measuring reversible photoconversion. A 405 nm laser is used for converting the same three ROIs previously activated. The laser powers are respectively 0.02 μW, 0.04 μW and 0.35 μW. 60 frames were acquired. For simplicity only six frames are shown (bottom) with the respective color selection indicated in the spectral phasor plot.

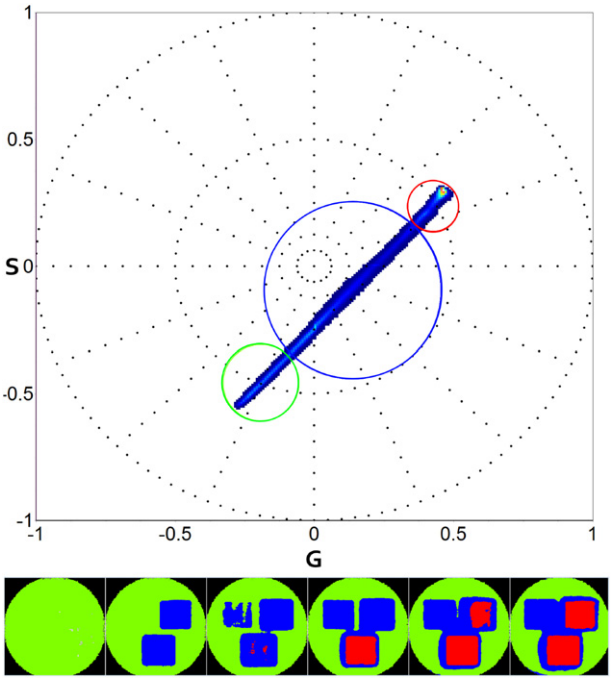

Figure 5. Kaede green to red photo-activation second harmonic spectral phasor analysis (top). Three ROIs are selected on the bead (53 pixels × 48 pixels). The laser power at 405 nm is set respectively at 0.04 μW (left ROI), 1.33 μW (right ROI) and 2.69 μW (bottom ROI). The zoom is set at 3.1 with a frame size of 43.06 μm × 43.06 μm. 100 frames are acquired using 488 and 561 nm wavelengths. The green cursor on the spectral phasor plot (top) is used to select the green state, the red cursor for the red state. The blue selection outlines the linear combination between green and red in the same pixel. In the image, pixels are colored according to the cursor color. We show six out of 100 frames acquired.

cluster selected by the green cursor highlights the green state of the PA-FP (green). The pixels undergoing photo-activation move to dark state values becoming undistinguishable from the background. When some proteins reach the dark state, phasors are shifted toward the center of the phasor plot, depending on the fraction of dark and fluorescent proteins in a pixel. We show the complete set of intensity images for Dronpa to underline the progression and completeness of photoconversion. The spectral graphs in figures 2 and 3 show the evolution of the signal over time in one of the regions of interest beginning from the green cursor selected points (in green) to progressively darker values (blue and red spectra). The decrease of the intensity and broadening of the full width at half maximum of the spectra correspond to points in the spectral phasor plot increasingly closer to the origin. These points correspond to the dark background and are not represented.

The same sample as in figure 2 is also used for imaging the kindling property of Dronpa. The same three ROIs are illuminated with the 405 nm laser and imaged at 488 nm to observe conversion from the 'dark' state to the fluorescent state. As expected from equations (1) and (2), the spectral phasor plot is analogous to the inactivation shown in figure 2. This demonstrates the capability of spectral phasors to fingerprint the activation state of photochromic proteins.

4. Kaede

Kaede at 29.09 mg ml^{-1} concentration is imaged using 488 nm and 561 nm lasers for exciting the green and red states respectively. Conversion is performed on three ROIs using a 405 nm laser at three different intensities. The second harmonic analysis of a 100 spectral image time series is shown in figure 5. Green and red states are identified at the extremes of the plot and marked using the matching color cursor. The linear combination pixels are marked in blue.

4.1. KikGR

Following the same protocol, we imaged KikGR at a concentration of 2.11 mg ml^{-1}. Photo-activation is mapped during 50 frames. Similarly to Kaede, the second harmonic phasor plot of KikGR (figure 6) shows points distributed along the linear combination of green and red states. The red state of KikGR peaks at 593 nm whereas that for Kaede is at 582 nm. Given the resolution attainable with the spectral phasor approach, which is a few nanometers, we could not expect to distinguish the KikGR phasor location from that of Kaede. Figure 7 shows the two PA-FP phasor distributions on the same plot. The two green states are too close to one another, as reported in the literature, with values of the green

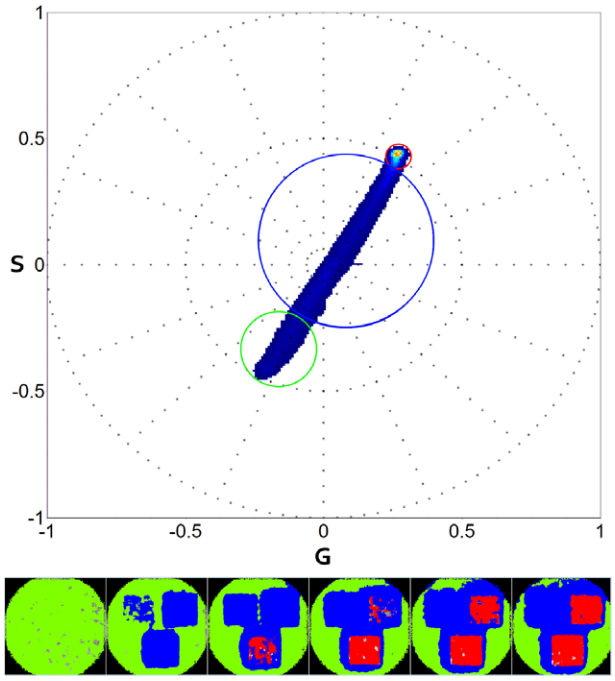

Figure 6. KikGR green to red photo-activation second harmonic spectral phasor analysis (top). Three ROIs are selected on the bead yielding 65 pixels × 68 pixels. Laser power at 405 nm is set respectively at 0.04 μW (left ROI), 1.33 μW (right ROI) and 2.69 μW (bottom ROI). The zoom is set at 2.0 with a frame size of 66.10 μm × 66.10 μm. 50 frames are acquired using 488 and 561 nm wavelengths. The green cursor on the spectral phasor plot (top) is used to select the green state, the red cursor for the red state. The blue selection outlines the linear combination between green and red. Corresponding frame pixels are colored according to the cursor color (bottom). For clarity we show six out of 50 frames acquired.

Table 1. Kaede–KikGR mixed sample fractional values from equation system (4). The relative brightness (RB) of the two proteins for each mixture is reported. The excitation wavelength is 561 nm. Emission is collected with the Zeiss 32 channel detector.

Fraction	Kaede	KikGR	Unconverted	Relative brightness
f_1	0.210	0.740	0.050	3.51
f_2	0.330	0.600	0.070	3.63
f_3	0.449	0.511	0.040	3.41

state for Kaede 518 nm (Ando *et al* 2002) and for KikGR 517 nm (Tsutsui *et al* 2005). In contrast, the red state is well separated on the second harmonic phasor plot (figure 7). The KikGR photo-active state is located at higher wavelength compared to that of Kaede, reflecting the values reported in the literature of 593 nm for KikGR (Tsutsui *et al* 2005) and 582 nm for Kaede (Ando *et al* 2002).

4.2. Mixture of PA-FPs

Next we exploit the diversity of two PA-FP spectral phasor distributions to resolve a mixture of photo-activatable proteins and to determine the relative molecular brightness of the different species. We diluted the protein solution fivefold

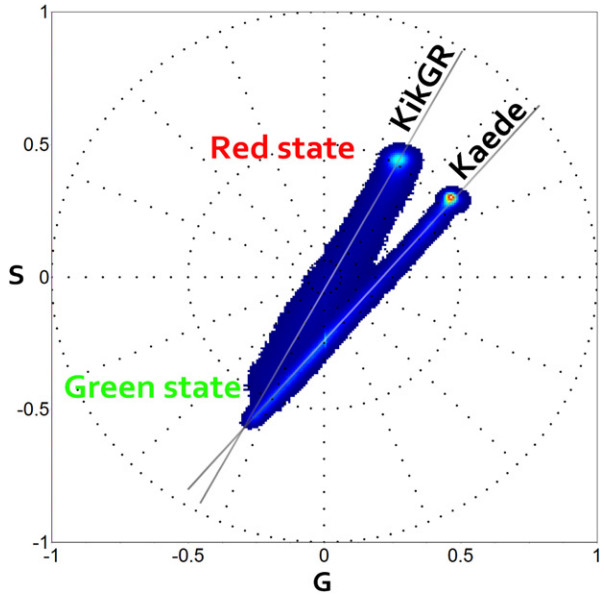

Figure 7. Second harmonic spectral phasor plot overlapping Kaede and KikGR distributions. The datasets used in figures 5 and 6 are here represented on the same phasor for comparison. The green state of both proteins originates from a similar emission wavelength as reported in the literature (Kaede/KikGR 518 nm/517 nm). The red state instead has different emission wavelengths for the two proteins.

and prepared three samples by mixing Kaede–KikGR first and adding the Ni-NTA agarose beads afterward. The three samples yielded a concentration ratio of Kaede–KikGR of respectively 3:1, 2:1 and 1:1. The resulting spectral phasor plots are shown in figure 8.

The three ratios overlap in the green state and separate in the red state. For reference we superimposed the spectral position of Kaede and KikGR. The mixed sample with 3:1 concentration is shifted toward the position of Kaede while the 1:1 is closer to the KikGR position. However, the mixed samples are not simply the linear combination of the red spectrum of the Kaede and KikGR. According to the linear combination rule for phasors, the only explanation of this effect is that there is an interaction between the two proteins or a third component that contributes to the mixture. One obvious candidate for this third component is a green component due to a noncomplete conversion from green to red. Using the linear combination law of phasors we can determine the amount of unconverted protein.

The equations describing the system (linear combination of three phasors) are given below (equation (4)). In these equations we use the vector law of addition separately on the g and s coordinates of the mixtures. There are nine unknowns, the fraction of the two proteins in the three mixtures and the fraction of unconverted protein, which we assume is the same for all samples. The values found for the unknown are given in table 1. The cumulative percentages of unconverted protein, mixed Kaede and KikGR, are 4%, 7% and 5% for 1:1, 2:1 and 3:1 ratios respectively.

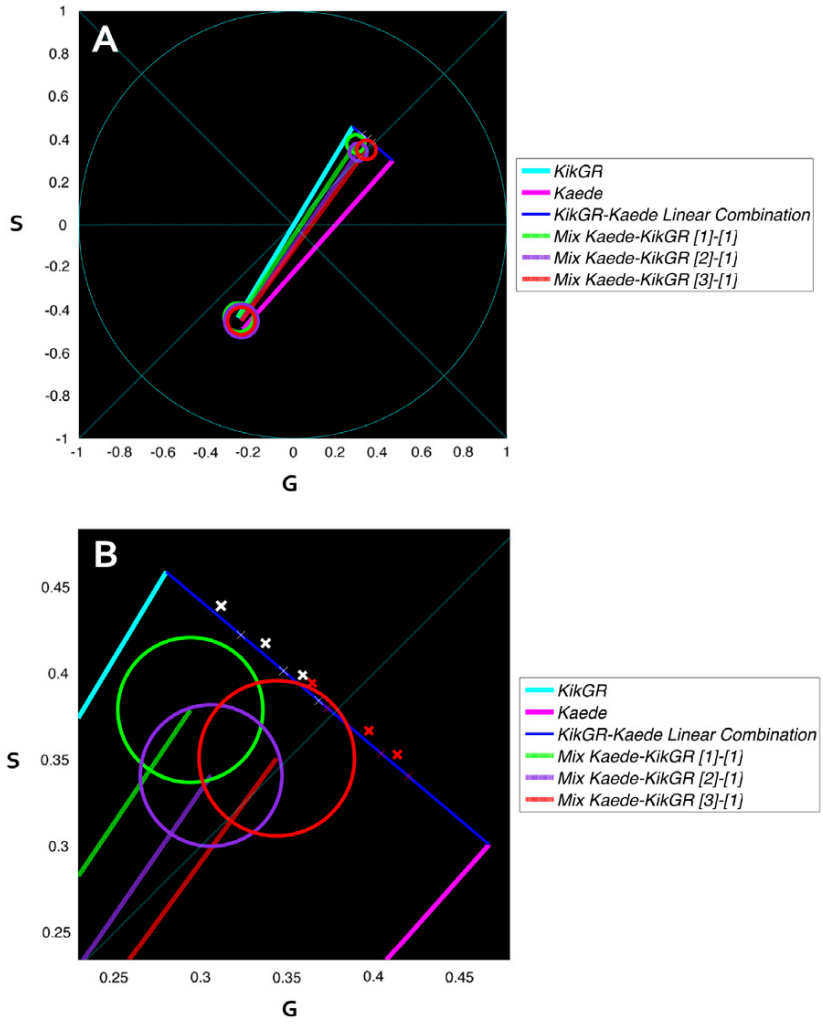

Figure 8. Second harmonic representation of three mixed Kaede–KikGR samples with concentration ratios 1:1 (green), 2:1 (purple) and 3:1 (red). Three sets of images were acquired using 488 and 561 nm laser lines. Each set has had three ROIs selected yielding approximately 63 pixels × 61 pixels. 50 images per sample were used for analysis. Cursors were placed selecting at least 90% of the pixels belonging to the specific state. (A) KikGR (light blue) and Kaede (violet) are represented. (B) Magnification of (A). A linear combination of red Kaede (violet) and KikGR (light blue) of mixtures with a relative brightness of 1 (red crosses) is shown in the line connecting the phasor of Kaede and KikGR. The measured intersections are shown in the white crosses on the same lines.

$$
\begin{aligned}
G_{\mathrm{mix1}} &= f_{1\mathrm{Kaede}} g_{\mathrm{Kaede(red)}} + f_{1\mathrm{KikGR}} g_{\mathrm{KikGR(red)}} \\
&\quad + f_1 g_{\mathrm{Kaede(green)}} \\
G_{\mathrm{mix2}} &= f_{2\mathrm{Kaede}} g_{\mathrm{Kaede(red)}} + f_{2\mathrm{KikGR}} g_{\mathrm{KikGR(red)}} \\
&\quad + f_2 g_{\mathrm{Kaede(green)}} \\
G_{\mathrm{mix3}} &= f_{3\mathrm{Kaede}} g_{\mathrm{Kaede(red)}} + f_{3\mathrm{KikGR}} g_{\mathrm{KikGR(red)}} \\
&\quad + f_3 g_{\mathrm{Kaede(green)}} \\
S_{\mathrm{mix1}} &= f_{1\mathrm{Kaede}} s_{\mathrm{Kaede(red)}} + f_{1\mathrm{KikGR}} s_{\mathrm{KikGR(red)}} \\
&\quad + f_1 s_{\mathrm{Kaede(green)}} \\
S_{\mathrm{mix2}} &= f_{2\mathrm{Kaede}} s_{\mathrm{Kaede(red)}} + f_{2\mathrm{KikGR}} s_{\mathrm{KikGR(red)}} \\
&\quad + f_2 s_{\mathrm{Kaede(green)}} \\
S_{\mathrm{mix3}} &= f_{3\mathrm{Kaede}} s_{\mathrm{Kaede(red)}} + f_{3\mathrm{KikGR}} s_{\mathrm{KikGR(red)}} \\
&\quad + f_3 s_{\mathrm{Kaede(green)}} \\
1 &= f_{1\mathrm{Kaede(red)}} + f_{1\mathrm{KikGR(red)}} + f_1 \\
1 &= f_{2\mathrm{Kaede(red)}} + f_{2\mathrm{KikGR(red)}} + f_2 \\
1 &= f_{3\mathrm{Kaede(red)}} + f_{3\mathrm{KikGR(red)}} + f_3.
\end{aligned}
\tag{4}
$$

The same linear combination rule excludes, in this case, the presence of an intermediate state. To demonstrate this we simulate two sets of data where an intermediate state appears. The resulting second harmonic spectral phasor plots are reported in figure 9. The first simulation (figure 9(A)) shows a first state at 503 nm, an intermediate state at 533 nm and an activated state at 591 nm. The second simulation shows an intermediate state close to the activated state, starting at 523 nm, an intermediate state at 571 nm and a final state at 581 nm. The hypothesis in these simulations is a complete conversion and an obligatory intermediate state before reaching the final activation. The resulting plot differs from the one obtained experimentally in figure 8, excluding the presence of intermediate states in our sample.

The linear combination rule of phasors also provides information on the brightness ratio between the red states of the two proteins. To use the set of linear equations, we measured the coordinates of the center of the distribution

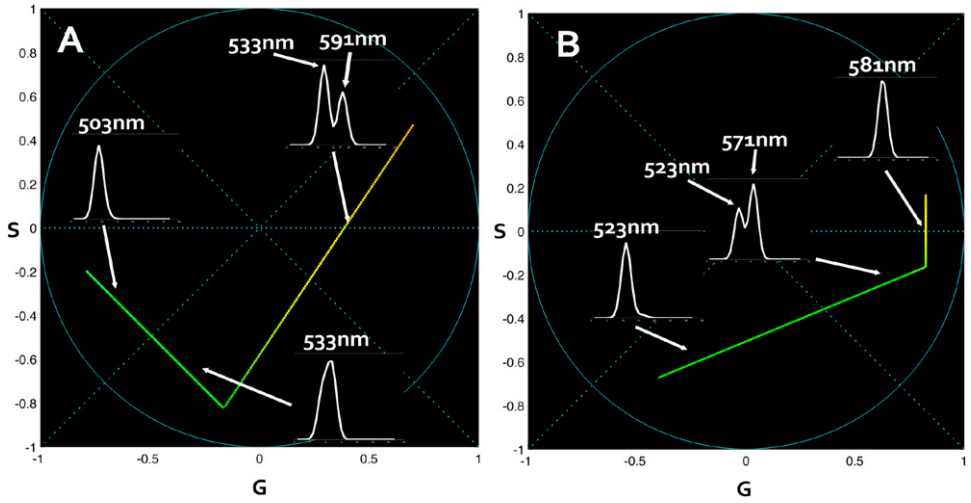

Figure 9. Second harmonic spectral phasor of intermediate-state simulated data. In these simulations we consider 100% conversion and an obligatory conversion to an intermediate state before reaching the final wavelength. Two sets are represented. The first set (A) shows a first state at 503 nm, an intermediate state at 533 nm and an activated state at 591 nm. The second set (B) shows an initial state at 523 nm, an intermediate state at 571 nm and a final state at 581 nm. Spectrum plots are reported on the image with an arrow indicating the corresponding position on the spectral phasor plot. The color scale in use associates the real color with the wavelength.

corresponding to Kaede and KikGR species from figures 5 and 6 and for the mixtures in figure 8. Solving the systems of linear equations provides the nine unknown values reported in table 1.

Note that in the equations above the fractions are fractional intensities, i.e., how much each species contributes to the spectral intensity. We are interested in comparing these values with the molar fractions of our preparations, so that we can obtain the relative molecular brightness of the various species. To solve this problem we need to know the molar fraction of the two proteins. We re-measure the diluted concentrations with the Bradford assay method, obtaining 1.27, 0.85 and 0.42 mg ml^{-1} for Kaede. The KikGR concentration was constant in the samples at 0.42 mg ml^{-1}. Applying the above values to the three ratio samples shows that KikGR has a higher brightness than Kaede. We calculate the relative molecular brightness as

$$\text{relative brightness} = \frac{[C]_{\text{Kaede}}}{[C]_{\text{KikGR}}} \frac{f_{n\text{KikGR}}}{f_{n\text{Kaede}}} \tag{5}$$

where C is the concentration and fractions $f_{n\text{Kaede}}$ and $f_{n\text{KikGR}}$ are obtained by solving system (4).

The resulting average brightness ratio for the red state of the KikGR–Kaede mixture is 3.52. The value itself is different from the literature (Tsutsui *et al* 2005). However, in our case two points need to be noted.

First, the excitation wavelength used for the red channel is 561 nm for both proteins. This wavelength differs from the excitation peak of Kaede (572 nm) (Ando *et al* 2002) and KikGR (583 nm) (Tsutsui *et al* 2005) and provides respectively 65.4% and 43.1% excitation efficiency.

Second, the Zeiss multispectral detector has not been corrected for different wavelength efficiencies.

These factors have a role in the measured brightness ratio and could explain the difference from the literature.

5. Conclusion

In this work we present an application of the spectral phasor approach to photo-activatable proteins using the second harmonic. The proteins chosen for this application are Dronpa, Kaede and Kikume Green-Red, representing a range of reversible photo-switchable and irreversible photo-activatable proteins. Our results demonstrate the possibility to distinguish PA-FPs during their photoconversion by their distribution in the phasor plot. We can easily determine in the phasor plot the initial and final states of the protein. Intermediate points are linear combinations of these states and therefore located on the line connecting the base to the photo-activated state.

We show a spectral phasor plot of mixed Kaede–KikGR samples with known concentration ratio. We can expect, in general, that if at least one of the states of the proteins is separated from the other by a few nanometers, the second harmonic analysis will distinguish different concentration ratios of these samples. Using simple linear algebra we can calculate the relative brightness ratio of the two proteins under these specific acquisition conditions.

The spectral phasor approach is ideal for imaging applications. The spectral phasor analysis proves to be a robust method for analysis of large datasets. The image sets acquired here reach 100 units with 32 channels, hence 3200 spectral frames carrying information. Calculating the spectral phasor is relatively fast and the results displayed in the phasor plot convey graphical information about the number of states (including intermediate states). Analysis is simplified and interpretation requires no particular expertise. A main advantage of this method resides in the global analysis: one single phasor plot could represent a large number of spectral images.

Acknowledgments

The authors would like to acknowledge Atsushi Miyawaki from the Laboratory for Cell Function Dynamics, Brain Science Institute, RIKEN, for providing the plasmids of Dronpa, Kikume Green-Red and Kaede, and Andrea Anzalone and Milka Stakic from the Laboratory for Fluorescence Dynamics, University of California Irvine, for helping optimize the protein purification protocol. This work was supported by grant numbers NIH-P41-RRO3155, P41-GM103540 and P50-GM076516.

References

Ando R, Hama H, Yamamoto-Hino M, Mizuno H and Miyawaki A 2002 An optical marker based on the UV-induced green-to-red photoconversion of a fluorescent protein *Proc. Natl Acad. Sci. USA* **99** 12651–6

Ando R, Mizuno H and Miyawaki A 2004 Regulated fast nucleocytoplasmic shuttling observed by reversible protein highlighting *Science* **306** 1370–3

Betzig E, Patterson G H, Sougrat R, Lindwasser O W, Olenych S, Bonifacino J S, Davidson M W, Lippincott-Schwartz J and Hess H F 2006 Imaging intracellular fluorescent proteins at nanometer resolution *Science* **313** 1642–5

Celli A, Sanchez S, Behne M, Hazlett T, Gratton E and Mauro T 2010 The epidermal Ca(2+) gradient: measurement using the phasor representation of fluorescent lifetime imaging *Biophys. J.* **98** 911–21

Chudakov D M, Matz M V, Lukyanov S and Lukyanov K A 2010 Fluorescent proteins and their applications in imaging living cells and tissues *Physiol. Rev.* **90** 1103–63

Digman M A, Caiolfa V R, Zamai M and Gratton E 2008 The phasor approach to fluorescence lifetime imaging analysis *Biophys. J.* **94** L14–6

Fereidouni F, Bader A N and Gerritsen H C 2012 Spectral phasor analysis allows rapid and reliable unmixing of fluorescence microscopy spectral images *Opt. Express* **20** 12729–41

Giral H, Lanzano L, Caldas Y, Blaine J, Verlander J W, Lei T, Gratton E and Levi M 2011 Role of PDZK1 protein in apical membrane expression of renal sodium-coupled phosphate transporters *J. Biol. Chem.* **286** 15032–42

Giral H *et al* 2012 NHE3 Regulatory Factor 1 (NHERF1) modulates intestinal sodium-dependent phosphate transporter (NaPi-2b) expression in apical microvilli *J. Biol. Chem.* **287** 35047–56

Habuchi S, Ando R, Dedecker P, Verheijen W, Mizuno H, Miyawaki A and Hofkens J 2005 Reversible single-molecule photoswitching in the GFP-like fluorescent protein Dronpa *Proc. Natl Acad. Sci. USA* **102** 9511–6

Habuchi S, Dedecker P, Hotta J, Flors C, Ando R, Mizuno H, Miyawaki A and Hofkens J 2006 Photo-induced protonation/deprotonation in the GFP-like fluorescent protein Dronpa: mechanism responsible for the reversible photoswitching *Photochem. Photobiol. Sci.* **5** 567–76

Hinde E, Digman M A, Welch C, Hahn K M and Gratton E 2012 Biosensor Forster resonance energy transfer detection by the phasor approach to fluorescence lifetime imaging microscopy *Microsc. Res. Tech.* **75** 271–81

Sanchez S, Bakas L, Gratton E and Herlax V 2011 Alpha hemolysin induces an increase of erythrocytes calcium: a FLIM 2-photon phasor analysis approach *PLoS One* **6** e21127

Stringari C, Cinquin A, Cinquin O, Digman M A, Donovan P J and Gratton E 2011 Phasor approach to fluorescence lifetime microscopy distinguishes different metabolic states of germ cells in a live tissue *Proc. Natl Acad. Sci. USA* **108** 13582–7

Stringari C, Sierra R, Donovan P J and Gratton E 2012 Label-free separation of human embryonic stem cells and their differentiating progenies by phasor fluorescence lifetime microscopy *J. Biomed. Opt.* **17** 046012

Tsutsui H, Karasawa S, Shimizu H, Nukina N and Miyawaki A 2005 Semi-rational engineering of a coral fluorescent protein into an efficient highlighter *EMBO Rep.* **6** 233–8